# A Scalable Variable Stiffness Revolute Joint based on Layer Jamming for Robotic Exoskeletons

Matthew Shen[0000−0002−9315−2737], Angus B. Clark[0000−0001−9662−6144], and Nicolas Rojas[0000−0001−5988−9180]

REDS Lab, Dyson School of Design Engineering, Imperial College London, 25 Exhibition Road, London, SW7 2DB, UK
(matthew.shen17, a.clark17, n.rojas)@imperial.ac.uk
http://www.imperial.ac.uk/reds-lab

**Abstract.** Robotic exoskeletons have been a focal point of research due to an ever-increasing ageing population, longer life expectancy, and a desire to further improve the existing capabilities of humans. However, their effectiveness is often limited, with strong rigid structures poorly interfacing with humans and soft flexible mechanisms providing limited forces. In this paper, a scalable variable stiffness revolute joint is proposed to overcome this problem. By using layer jamming, the joint has the ability to stiffen or soften for different use cases. A theoretical and experimental study of maximum stiffness with size was conducted to determine the suitability and scalablity of this technology. Three sizes (25 mm, 18.75 mm, 12.5 mm diameter) of the joint were developed and evaluated. Results indicate that this technology is most suitable for use in human fingers, as the prototypes demonstrate a sufficient torque (0.054 Nm) to support finger movement.

**Keywords:** Variable Stiffness · Layer Jamming · Exoskeleton.

## 1 Introduction

Robotic exoskeletons have been a recent focus of robotics research due to rise of areas such as power augmentation and rehabilitation robotics. Robotic exoskeletons are advantageous as they combine the strength of robots and dexterity and control of humans to create a man-machine system which is more intelligent than a robot, but also more powerful than a human [8]. In recent years, the majority of research into robotic exoskeletons has focused on creating a rigid frame which the user is strapped onto to reduce the strain on the user when a large torque is applied by the exoskeleton [7]. Although a rigid exoskeleton can provide extra structural integrity to the man-machine system, multiple rotary joints may also cause loss of degrees of freedom (DOF) in certain configurations [13]. Misalignment of the exoskeleton and human joints can also result in inaccuracies in measurements as well as applying unergonomic forces upon the user.

(a) (b) (c)

**Fig. 1.** The developed variable stiffness joints based on layer jamming technologies at three radii:**(a)** 25 mm, **(b)** 18.75 mm, and **(c)** 12.5 mm.

Solutions to these problems have already been proposed, but are at the cost of increased mechanical complexity [4] [16].

An alternative approach is to utilise soft wearable robotics which are less bulky and do not need to be aligned to each user as accurately as their rigid counterparts. In general, soft exoskeletons are used in cases where the user requires assistance to carry out daily tasks which are not intensive. Researchers have developed different forms of wearable exoskeletons to suit different purposes [9] [15]. Soft exoskeletons can also no longer be actuated using motors that require a rigid framework, instead, tendons and artificial muscles are most commonly used in these devices. A downside of soft exoskeletons are that they are inherently controlled by tension, which loses the ability of holding a certain position rigidly. This is a necessary function to protect joints of the user in cases of rehabilitation.

A solution to this is to improve current soft wearable exoskeletons by using elements from continuum robots, which are variable stiffness limb segments that can be reconfigured to suit the user's needs [6] [12]. If a variable stiffness element can be incorporated into designs of current soft exoskeletons, advantages of a soft exoskeleton can be preserved while ensuring sufficient protection to the joints when required. Currently, the most reliable continuum robots achieve variable stiffness using one of two mechanical methods: layer-jamming and granular-jamming [5] [10] [11]. Both of the above-mentioned technologies rely on applying pressure to increase friction between mechanical objects to control the stiffness of the overall limb. However, layer-jamming is advantageous over granular-jamming due to a smaller volume required, a lighter weight as well as being hollow [6]. In the case of an exoskeleton, the layer-jamming technology could be set up around the user's joints, in which its advantages allows it to be more suitable in creating a comfortable interface with human users.

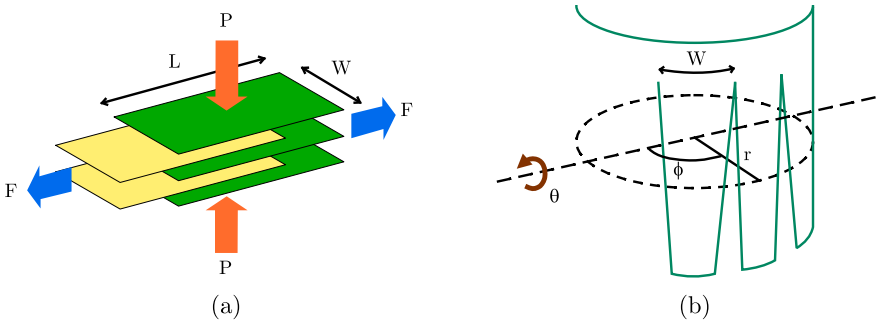


**Fig. 2. (a)** Layer jamming principle: With a pressure applied over stacked layers, force F is required to separate the layers and **(b)** schematic diagram outlining equation 2 parameters of the variable stiffness joint in relation to the revolute axis.

Kim et al. [11] described a design of a variable stiffness joint based on layer-jamming and activated using a vacuum pump, successfully demonstrating the effectiveness and feasibility of layer-jamming technologies. In their research, the 1 DOF variable stiffness joint was used as a proof of concept in the development of a snake-like manipulator with variable stiffness. In this paper, we leverage this design principle to implement a scalable variable stiffness joint by applying negative pressure to contract layers of Mylar films. We present a novel 1 DOF variable stiffness exoskeleton joint, differing from previous research which has focused on continuum robot implementations. As shown in Fig. 1, three prototypes were produced to measure the capabilities of the layer jamming technology at different scales. By investigating the operation of the variable stiffness joint under varying conditions, scaling of stiffness can be calculated. These results are useful to improve the design of soft exoskeletons to be used on joints of varying sizes on the human body.

The rest of this paper is organised as follows. In section II, the expected forces and stiffness of the joints are calculated and compared against scale. In section III, development and manufacturing details are discussed, with inclusion of consideration of specific design aspects. In section IV and V, results and trends are analysed and feasibility of use in soft exoskeletons are reviewed. Finally, conclusions and practicalities are discussed in section VI.

## 2 Theoretical Analysis

When looking at the effectiveness of a variable stiffness joint, the maximum stiffness of the joint is a good indicator. To evaluate the maximum stiffness in terms of a maximum resistive torque, the tensile strength of the layers must be considered, which can be expressed as the maximum static friction between the layer jamming layers:

$$F = \mu n P W L, \tag{1}$$

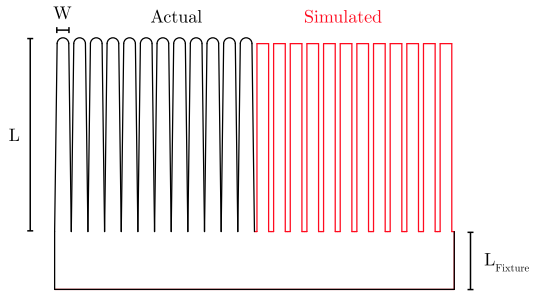


**Fig. 3.** Unwrapped singular Mylar layer, with actual design of the Mylar layer (left, black) and simulated Mylar layer used in calculation of total resistive torque (right, red).

where $\mu$ is the static coefficient of friction, n is the number of contact surfaces, P is the applied pressure in the normal direction, and W and L are the width and length of the layer jamming flaps respectively. This is shown in Fig. 2a.

It is to be noted that this is an approximation of the tensile strength which assumes that all the contact areas of the layers will 'slip' at exact the same moment. As the kinetic coefficient of friction is lower than the static coefficient of friction, this approximation will lead to an estimation of the tensile strength that is greater than reality.

Now, the maximum resistive torque can be considered. It is important to realise that the resistive torque that each of the flaps provides is dependent on the orientation of the flaps with respect to the rotational axis of the joint. The motion of overlapping flaps with normal axis parallel to the axis of rotation is purely rotational, while flaps with normal axis perpendicular have purely transnational motion. Flaps in between will naturally have contributions from both translational and rotational motion, resulting in challenging calculations.

Instead of considering both motions separately, Kim et al. has carried out the calculation through analysing the motion of a infinitesimal segment of the layers [11]. From this, Kim et al. was able to derive the maximum resistive torque as:

$$\tau(\phi) = p\mu w \left( \frac{L}{4} \sqrt{(L\cos\phi)^2 + (2r\sin\phi)^2} + \frac{(r\sin\phi)^2}{\cos\phi} \ln\left( \frac{L}{2r}\cot\phi + \sqrt{(\frac{L}{2r}\cot\phi)^2 + 1} \right) \right). \quad (2)$$

where $r$ is the radius of the jamming cylinder. It is seen from equation (2) that the resistive torque of each flap is a function of $\phi$, which is defined as the angle between the normal axis of the flaps and the axis of rotation of the joint, shown in Fig. 2b.

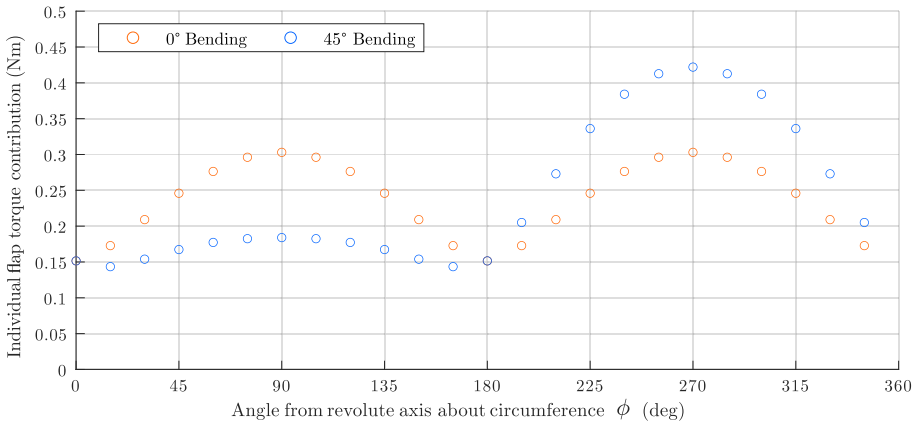


**Fig. 4.** Simulated torque contribution of the flaps at each orientation at bending angles of 0° (red) and 45° (blue) of the joint.

To extend this calculation to include the bending orientation of the joint, a modification of the effective overlapping length of the flaps can be imposed:

$$L'(\phi) = L + \Delta L_\theta(\phi) = L - \theta r sin(\phi), \tag{3}$$

where $\theta$ is the angle that defines the orientation of the joint. By replacing $L$ with $L'$ in equation (2), the resistive torque of a flap at any bending angle of the joint can be determined. From here, the total resistive torque can be calculated through summing the contributions of each flap in equation (2) to define a theoretical value of maximum resistive torque of the layer jamming joint.

The theoretical results of the individual flap contribution to the total torque with respect to the angle at which the flap is situated is modelled using the structure shown in Fig. 3 and results are shown in Fig. 4. The parameters used in this analysis are equivalent to the design parameters used in designing the largest prototype, namely $r = 25$ mm, $L = 40$ mm, $p = 80$ kPa, $\mu = 0.4$ and $w = 5$ mm. A total of 10 layers were used with 24 flaps in each layer. From Fig. 4, a symmetric contribution of torque can be seen as expected at 0° bending of the joint. On the other hand, at 45° bending, an asymmetric contribution is observed as a result of the modifications in effective overlapping length around the joint. Between angles 0° and 180°, a significant decrease in torque is the direct result of a decreased $L'$, whereas the opposite effect is observed between angles 180° and 360°.

Interestingly, the modification of an bending orientation as introduced by the inclusion of consideration of effective overlap in equation (3) has no effect on the total resistive torque, which remains a constant with varying $\theta$. This can be explained as the increase in overlap of a flap is exactly equivalent to the decrease of overlap in the flap directly opposite, resulting in a zero net effect on the total torque.

**Table 1.** Design parameters of the variable stiffness joints

| Radius (mm) | Length (mm) | L (mm) | W (mm) | $\tau_{total}$ (Nm) | Force (N) |
|---|---|---|---|---|---|
| 25 | 160 | 50 | 4.9 | 34.09 | 426.09 |
| 18.75 | 140 | 22.5 | 3.4 | 6.60 | 82.55 |
| 12.5 | 120 | 15 | 2.0 | 1.68 | 20.97 |

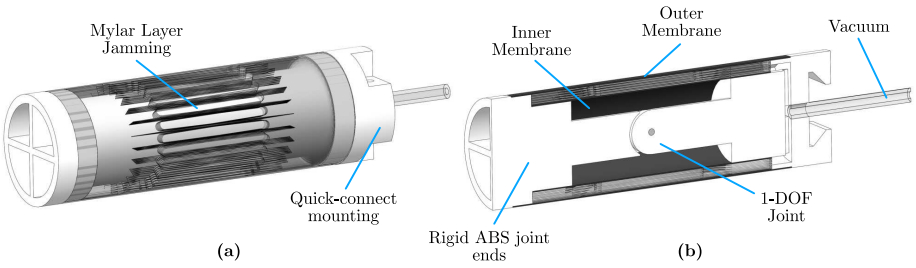


**Fig. 5.** CAD drawing of the designed variable stiffness joint (25 mm design): **(a)** Outer view showing overlapping layers and **(b)** cross sectional view showing internal structure.

Table 1 shows the results of the simulation of total torque and maximum rotational force that can be applied to the end of the joints. It would be expected that the scaling of the total force would be quadratic due to the quadratic scaling of surface area of the flaps with radius. However, the total torque seems to scale exponentially instead. This is non-physical and highlights the failures in simplifications of the model at large scales. A suggestion to improve this model is to derive the net torque based on each infinitesimal surface area instead of flap segment.

## 3 Development of Joint

The development of the joint was based off previous designs of layer jamming proposed by other authors [11] [12]. The basic setup consisted of circular layers of flaps which overlapped, encapsulated by two layers of membrane as seen in Fig. 5. By using a vacuum pump to generate a negative pressure between the layers, atmospheric pressure compresses the layers together to achieve layer jamming which stiffens the overall structure. Variable friction can then be fine tuned through control of the applied negative pressure, with a theoretical maximum of $-101.3$ kPa.

In this paper, three prototypes at different scales are presented, each with 24 flaps in each of the 10 Mylar (polyethyleneterephthalate film) layers, manufactured using a laser cutter. The end housing were 3D printed in acrylonitrile butadiene styrene (ABS) material, and connected to a vacuum pump via a 6 mm PVC tubing. The latex membrane were cut to required size by hand from a large sheet and formed into a tubular shape with adhesive; once dried, they were then

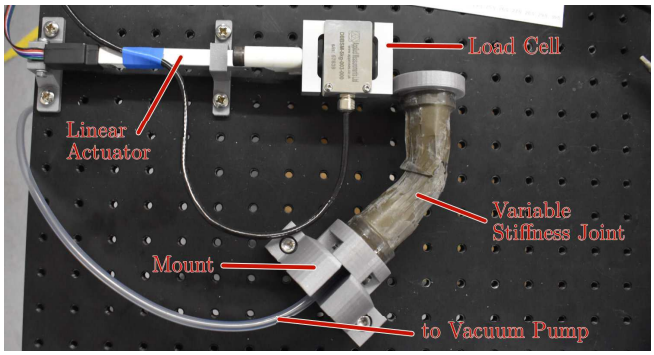


**Fig. 6.** Experimental setup for evaluating maximum resistive torque of the joint.

attached to the end housing to create the vacuum chamber. Specific design parameters of each prototype can be found in Table 1, where the smallest prototype of radius 12.5 mm was a limit as prototypes with smaller radius were too difficult to manufacture. The prototypes were created such that they shared the same base radius, ensuing fair and comparable results when mounting onto a test bed.

During development of the prototypes, design parameters were specified with respect to the chosen radius of the central joint and a desired maximum bending angle (45°). All parameters follow the principle of minimising the overall structure without compromising functionality. By defining the central radius and maximum bending angle, the overall length of the joint is determined by considering the amount of room required for the Mylar layers to slide across each other with a minimum overlap of $2r$ for each flap at the maximum bending angle. Following this calculation, the minimum length of the Mylar flaps are $2r + \frac{3}{2}\theta_{max}r$, which defines the minimum length of the whole joint to be $2(r + \theta r)$. The radius of the inner membrane was also chosen with consideration of the thickness of each layer to ensure they can be contained within the membranes.

## 4 Experimental Evaluation

### 4.1 Experimental Setup

To evaluate the performance of the layer jamming joints at varying operational parameters, the test setup shown in Fig. 6 was used. The test-bed was based on an optical bench with threaded holes of 6mm diameter spaced in a square lattice of 25 mm separation between adjacent holes. Housing for each of the components were created and 3D printed in ABS material to match the spacing on the bench.

The tests conducted focused solely on the stiffness of the joint, which was measured using a load cell(DBBSM 5kg) connected to a linear actuator (Actuonix L12-100-100-12-I). Each test would consist of the linear actuator pressing the load cell 10 mm into the end of the variable stiffness joint to measure the

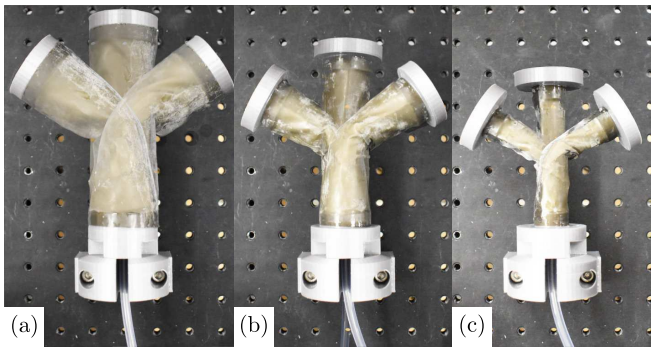


**Fig. 7.** Bending capabilities of the developed variable stiffness joints of radius 25 mm **(a)**, 18.75 mm **(b)**, and 12.5 mm **(c)**.

maximum resistive force. From the force experienced by the load cell, the length of the joint was used to calculate the resistive torque exerted by the joint. Readings were acquired using a NI DAQ (LabView 6211), from which the maximum reading of force was extracted from the measured data.

For each of the three joints created, tests were conducted in 3 orientations: clockwise push at 0° (upright) and −45°, and anticlockwise push at 45°. The three positions for each of the joints are shown in Fig. 7. Negative pressure levels of $0 - 80$ kPa were tested in increments of 20 kPa for each joints at each orientation. It is noted that due to the natural springiness of the joints, tests at 0 kPa could only be conducted at the 0° orientation as the joints cannot hold its orientation at 45° and −45° when no pressure is applied. To ensure reliable results, the pressure and orientation of the joints were reset between each repeat measurement by turning off the vacuum pump and moving the joint across its whole range before setting it into the desired orientation.

### 4.2 Results

The results of the experiment are shown in Fig. 8, confirming the increase of stiffness with pressure in most scenarios. The 9 sets of data do not show a clear linear trend between pressure and total torque as predicted, and fluctuations indicate large margin of errors in the collected data. The maximum torques observed for the 25 mm, 18.75 mm and 12.5 mm were 0.216 Nm, 0.138 Nm and 0.054 Nm respectively.

Results also indicate an overall increase in stiffness with radius as expected. However, no conclusive trend of stiffness against scale can be observed from the results gathered.

Comparing the three orientations, it is seen that the 0° orientation provided the highest stiffness out of the three examined orientations, which differs from the simulated results where bending angle does not result in a net effect. Further comparing results from the −45° and 45° orientation, it is observed that the two

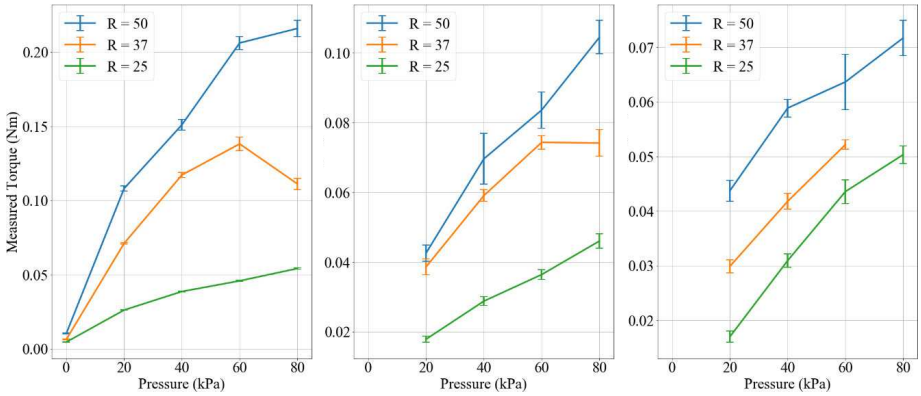


**Fig. 8.** Maximum resistive torque of the variable stiffness joints under different vacuum pressures and orientations: **(a)** 0° pushing clockwise, **(b)** −45° pushing clockwise, and **(c)** 45° pushing anticlockwise.

sets of data do not correlate well. This is unexpected as the joints were designed to be symmetric, which suggests that the results should also be symmetric across bending angles.

The measurement of the anticlockwise push at −80 kPa is not measured due to a leakage in the $r = 18.75$ mm joint which prevents the vacuum pump from reaching the desired pressure. The other points of the $r = 18.75$ mm joint at −80 kPa also exhibit unexpected results, with a decrease of stiffness at 0° and −45° orientations from its previous point.

Comparing the measured results with the simulated values, the simulated values are all substantially higher than the measured values, with the simulated value at $r = 25$ mm being 2 degrees of magnitude higher than the measured value. This discrepancy is discussed further in the section below.

In Fig. 9, an implementation of the joint used as a restrictive elbow exoskeleton is seen. This use case would be most suitable for users with injured elbows, biceps or triceps, in which the stiffening capabilities will support the user's muscles in maintaining a desired elbow orientation.

## 5 Discussion

Specific trends cannot be extracted from the measured results, and correlation between measured datasets at different radii are not observed across the pressure range. This emphasises the great margin of systematic error seeing as the standard error of the measurement does not encompass the range of fluctuation of the measured data. There are three potential causes of systematic error and their effects are discussed below.

(a) (b) (c)

**Fig. 9.** The developed variable stiffness joint implemented as a restrictive elbow exoskeleton: **(a)** Variable stiffness off with arm bent, **(b)** Variable stiffness on with arm bent, and **(c)** Variable stiffness off with arm straight.

Firstly, structural deformation of the layer jamming structure due to high pressures will cause the recorded stiffness of the structure to decrease. This occurs when the pressure applied by the membranes on the Mylar layers causes them to buckle and lose structural integrity, which allows the joint to bend without the Mylar layers sliding across each other at all. The effect of this is most clearly seen for the $r = 18.75$ mm joint, where an increase in pressure from 60 kPa to 80 kPa has not increased the stiffness at the tested orientations.

Another source of significant systematic error is the inconsistencies in the manufacturing process. To ensure that results are comparable, the joints are designed to scale proportionally. However, during the lengthy process of manufacturing, alignment of each of the parts with respect to another cannot be ensured to perfection. This results in an increase in the spread of the measured results, and also provides an explanation to the observed asymmetry in results of the clockwise and anticlockwise orientations.

A persistent source of error may be caused by leakages of the inner membrane. As maximum reachable pressures of each of the joints decrease over the experimental process, it is clear that punctures in the outer membrane are developing. Leakages in the outer membrane do not affect measured results as long as the barometer indicates the desired pressure reading. However, leakages in the outer membrane also indicate the possibility of punctures in the inner membrane, which could be problematic. This is because in the design of the joints, the volume within the inner membrane is also sealed air-tight, if a leakage exists, the effective vacuum would extend to within the inner membrane. As a result, only the outer membrane would provide pressure onto the layers, which would substantially decrease the observed resistive torque of the joints.

Discrepancies between the simulated values and the measured values can be explored in three respects. At non-zero bending angles, the Mylar cylinders deform and are no longer exactly circular, which causes structural deformation that causes a reduction of torque. This may explaine to how the bending angle influences overall torque. Next, the simulation assumes that all of the layers

slip at the same time. Since static friction is larger than kinetic friction, this assumption will cause the force estimated to be greater by up to a factor of $\mu_{static}/\mu_{kinetic} \approx 2$. Lastly, the model supposes that bending of the joint can only be allowed through slipping of the layers, which is not always the case. If the structural strength of the Mylar cylinder is weaker than the resistive strength of the Mylar friction, the structure may bend under buckling of the layers, which will cause a lower observed torque.

Relating the measured results to physical parameters of the human body. The average human finger (middle) has a diameter of 23.2 mm (male) and 20.4 mm (female), wrist with a diameter of 55.7 mm (male) and 49.0 mm (female) [1]. These values are comparable to the 12.5 mm and 12.5 mm joints presented in this paper. In activities of daily living, the amount of force required by the proximal interphalangeal (PIP) joint in the finger ranges from $\sim 1.8 - 43.5$ N [3]. This corresponds to a minimum torque of 0.004 Nm, which is within the range of resistive torque the 12.5 mm joint can provide at 80 kPa [2]. This comparison suggests that the design is suitable for use in robotic finger exoskeletons in its current state.

On the other hand, torque required by the wrist for activities of daily living are estimated to be 8.62 Nm (male) and 5.20 Nm (female) [14]. This is significantly higher than the maximum torque of 0.22 Nm supplied by the 25 mm joint, making this version of the variable stiffness joint unsuitable for use in the wrist.

## 6 Conclusion

In this paper three variable friction joints at radii of 12.5 mm, 18.75 mm and 25 mm were manufactured to explore the scalability of layer jamming joints and their uses in soft robotic exoskeletons. The maximum stiffening capabilities of the joints were measured in three orientations: $0°$ and $-45°$ bending angle pushing clockwise, and at $45°$ bending angle pushing anticlockwise. At each orientation, the joints were measured at pressures of $0 - 80$ kPa in increments of 20 kPa to investigate the overall trend.

The joints demonstrated maximum resistive torques of 0.216 Nm, 0.138 Nm and 0.054 Nm for the 25 mm, 18.75 mm and 12.5 mm joints, respectively. Algebraic trends of the prototypes are not observed with respect to scale or pressure from the results due to large margin of systematic errors. From comparing the maximum resistive torques, this technology in its current form is most suited for use in robotic exoskeletons for the human finger joint for support and protection for activities of daily living. Future work may explore manufacture techniques to further optimise the product as well as methods to increase resistive torque to enable usage in soft exoskeletons that support other joints of the human body.

## References

1. Bolton, C.F., Carter, K.M.: Human sensory nerve compound action potential amplitude: variation with sex and finger circumference. Journal of Neurology, Neuro-

surgery & Psychiatry **43**(10), 925–928 (1980)
2. Bundhoo, V., Park, E.J.: Design of an artificial muscle actuated finger towards biomimetic prosthetic hands. In: ICAR'05. Proceedings., 12th International Conference on Advanced Robotics, 2005. pp. 368–375. IEEE (2005)
3. Butz, K.D., Merrell, G., Nauman, E.A.: A biomechanical analysis of finger joint forces and stresses developed during common daily activities. Computer methods in biomechanics and biomedical engineering **15**(2), 131–140 (2012)
4. Carignan, C., Tang, J., Roderick, S.: Development of an exoskeleton haptic interface for virtual task training. In: 2009 IEEE/RSJ International Conference on Intelligent Robots and Systems. pp. 3697–3702. IEEE (2009)
5. Clark, A.B., Rojas, N.: Assessing the performance of variable stiffness continuum structures of large diameter. IEEE Robotics and Automation Letters **4**(3), 2455–2462 (2019)
6. Clark, A.B., Rojas, N.: Stiffness-tuneable limb segment with flexible spine for malleable robots. In: 2019 International Conference on Robotics and Automation (ICRA). pp. 3969–3975. IEEE (2019)
7. Frey, M., Colombo, G., Vaglio, M., Bucher, R., Jorg, M., Riener, R.: A novel mechatronic body weight support system. IEEE Transactions on Neural Systems and Rehabilitation Engineering **14**(3), 311–321 (2006)
8. Gopura, R., Kiguchi, K., Bandara, D.: A brief review on upper extremity robotic exoskeleton systems. In: 2011 6th international Conference on Industrial and Information Systems. pp. 346–351. IEEE (2011)
9. In, H., Kang, B.B., Sin, M., Cho, K.J.: Exo-glove: A wearable robot for the hand with a soft tendon routing system. IEEE Robotics & Automation Magazine **22**(1), 97–105 (2015)
10. Jiang, A., Xynogalas, G., Dasgupta, P., Althoefer, K., Nanayakkara, T.: Design of a variable stiffness flexible manipulator with composite granular jamming and membrane coupling. In: 2012 IEEE/RSJ International Conference on Intelligent Robots and Systems. pp. 2922–2927. IEEE (2012)
11. Kim, Y.J., Cheng, S., Kim, S., Iagnemma, K.: Design of a tubular snake-like manipulator with stiffening capability by layer jamming. In: 2012 IEEE/RSJ International Conference on Intelligent Robots and Systems. pp. 4251–4256. IEEE (2012)
12. Langer, M., Amanov, E., Burgner-Kahrs, J.: Stiffening sheaths for continuum robots. Soft robotics **5**(3), 291–303 (2018)
13. Lo, H.S., Xie, S.Q.: Exoskeleton robots for upper-limb rehabilitation: State of the art and future prospects. Medical engineering & physics **34**(3), 261–268 (2012)
14. Morse, J.L., Jung, M.C., Bashford, G.R., Hallbeck, M.S.: Maximal dynamic grip force and wrist torque: The effects of gender, exertion direction, angular velocity, and wrist angle. Applied Ergonomics **37**(6), 737–742 (2006)
15. Park, Y.L., Santos, J., Galloway, K.G., Goldfield, E.C., Wood, R.J.: A soft wearable robotic device for active knee motions using flat pneumatic artificial muscles. In: 2014 IEEE International Conference on Robotics and Automation (ICRA). pp. 4805–4810. IEEE (2014)
16. Stienen, A.H., Hekman, E.E., Van Der Helm, F.C., Van Der Kooij, H.: Self-aligning exoskeleton axes through decoupling of joint rotations and translations. IEEE Transactions on Robotics **25**(3), 628–633 (2009)